Magnetoelastic interactions in the series of rare-earth phosphates RPO_4 (R = Tb-Tm)

1999 J. Phys.: Condens. Matter 11 1289

(http://iopscience.iop.org/0953-8984/11/5/015)

J. Phys.: Condens. Matter **11** (1999) 1289–1304. Printed in the UK PII: S0953-8984(99)95347-X

Magnetoelastic interactions in the series of rare-earth phosphates RPO_4 (R = Tb–Tm)

P Morin† and Z Kazei‡

† Laboratoire Louis Néel, CNRS, 166X, 38042, Grenoble Cédex, France
‡ Laboratory for Magnetism, Physics Department, Moscow State University, 119899 Moscow, Russia

Received 22 June 1998, in final form 17 November 1998

Abstract. The magnetic and magnetoelastic properties of RPO_4 (R = Dy, Ho, Er), which have the zircon-type tetragonal structure, are investigated in the paramagnetic phase within the extended susceptibility formalism. The characteristic behaviour of the first-order magnetic susceptibility allows us to refine the values of the crystalline electric field parameters and to determine the strength of the magnetic interactions. The magnetoelastic coefficients and quadrupolar constants for all the symmetry-lowering modes are then determined from third-order magnetic susceptibility and parastriction measurements. Their coherency within the series of RPO_4 is emphasized: all the magnetoelastic couplings keep the same sign and order of magnitude; the tetragonal magnetoelastic coefficients are sizeable in comparison with those determined in the rare-earth intermetallics. The variation of the crystalline electric field interactions and of the magnetoelastic couplings throughout the series of RPO_4 (Tb–Tm) is discussed, which is an essential step towards a coherent understanding of the magnetic behaviour of the whole series.

1. Introduction

Rare-earth phosphates RPO_4 belong to the group of rare-earth (R) oxide compounds RXO_4 (X = As, P, V), which possess a tetragonal zircon structure (space group $I4_1/amd$) at room temperature; four equivalent R ions in a unit cell occupy sites of $\bar{4}2m$ (D_{2d}) point-group symmetry [1]. R zircons are known to be archetypal Jahn–Teller compounds, a number of which exhibit spontaneous tetragonal–orthorhombic transitions and have then motivated a great number of studies of the Jahn–Teller coupling [2]. It is now well established that the occurrence of the cooperative Jahn–Teller effect depends on both the strength of the magnetoelastic coupling and the strain susceptibility of the quadrupolar parameter liable to order; this susceptibility is ruled by the crystalline electric field (CEF) resulting from the surroundings of the 4f ions. The CEF mixing of the eigenfunctions is almost the same for R vanadates and arsenates, but changes drastically for R phosphates. This is due to the fact that the second-order CEF parameter, V_2^0, changes in sign in RPO_4, the other CEF parameters being almost unchanged [3]. Thanks to that, although the magnetoelastic couplings remain of the same order of magnitude in three isomorphous series, the magnetoelastic behaviours of R phosphates, in particular the conditions of occurrence of the cooperative Jahn–Teller effect, are quite different. In a more general way, the problem of the magnitude of the CEF and magnetoelastic interactions themselves in R zircons remains open and, for example, it is not clear why for other R oxides with tetragonal or lower crystal structure these interactions differ

0953-8984/99/051289+16$19.50

in such a way that the structural phase transitions either do not occur at all, as in R scheelites [4], or take place as an exception (as in $CsDy(MoO_4)_2$) [5].

Recently we have initiated the systematic studies of the magnetoelastic and quadrupolar interactions in the series of R phosphates. Two members of this series, $TbPO_4$ [6] and $TmPO_4$ [7], have been thoroughly studied in the frames of an extended magnetic and quadrupolar susceptibility formalism, which operates with the actual wave functions and level energies of the ground state multiplet [8]. This approach, based on perturbation theory in the disordered phase, allows one to determine, for all the symmetry lowering modes, both the one-ion magnetoelastic term and the quadrupolar pair interactions, starting from the ordinary (magnetic, magnetoelastic and elastic) experimental data. The knowledge of these different couplings combined with self-consistent diagonalization of the full Hamiltonian then allows the properties in the ordered phase or in high magnetic fields to be determined. In the two compounds, although none of the different symmetry-lowering modes can be completely neglected, the dominant magnetoelastic coupling is associated with the δ-orthorhombic symmetry. In $TbPO_4$, it is mainly responsible for the transition observed at 2.15 K; almost twice as large in $TmPO_4$, it is however unable to drive the Jahn–Teller transition owing to a non-favourable CEF configuration. The intermediate members of this series from Dy to Er do not exhibit quadrupolar interactions as large as in these two compounds, but their magnetoelastic properties are of evident interest to interpret coherently the magnetoelastic behaviour of the whole series.

In Dy and Ho phosphates, the R magnetic moments order antiferromagnetically along the c-axis at 3.4 and 1.4 K, respectively [9, 10]. The CEF mixing gives rise to highly anisotropic low-lying energy levels, which are responsible for large Ising-type behaviours. No magnetic ordering has been observed in $ErPO_4$ down to 0.4 K [11]. From neutron diffraction, optical absorption and Mossbauer effect studies, the ground state is known to have large $|15/2, \pm 15/2\rangle$ components in $DyPO_4$ and the separation between the lowest and the first excited states was determined to be about 100 K [12, 13]. Owing to a huge magnetic anisotropy, a metamagnetic phase transition can be induced below T_N by a magnetic field applied along the c-axis [14]. In the ordered state, a large magnetoelectric effect was observed in $DyPO_4$ [15]. Measurements of the magnetic susceptibility, magnetic moment and specific heat of holmium phosphate indicate that it is also highly anisotropic [10, 16, 17]. In contrast to Dy and Ho phosphates, in $ErPO_4$, the magnetic susceptibilities along the tetragonal axis and in the basal plane are comparable in magnitude below 10 K showing no apparent 'easy direction' for cooperative magnetization [18].

Thus, though RPO_4 with Dy, Ho and Er are not ruled by strong JT correlations such as in $TbPO_4$ or $TmPO_4$, they exhibit a number of interesting features and appear good candidates for an investigation using the susceptibility formalism. After a brief recall of this treatment in section 2 and a discussion of the CEF coupling (section 4), the determination of the various magnetoelastic couplings are presented in sections 5 and 6. The results will be discussed in section 7.

2. Formalism

The magnetic properties of the 4f shell are described for a tetragonal symmetry with the following Hamiltonian [8] using the operator equivalent method [19] and the mean field approximation (MFA):

$$H = H_{CEF} + H_M + H_{ME} + H_Q + (E_{el} + E_M + E_Q). \tag{1}$$

The CEF term, H_{CEF}, is written within a system of $x,\ y,\ z$ axes parallel to the [100], [010] and [001] axes of the lattice cell, respectively,

$$H_{CEF} = \alpha_J V_2^0 O_2^0 + \beta_J (V_4^0 O_4^0 + V_4^4 O_4^4) + \gamma_J (V_6^0 O_6^0 + V_6^4 O_6^4) \tag{2}$$

where O_m^1 are the Stevens operators, V_m^1 the CEF parameters, $\alpha_J,\ \alpha_J,\ \alpha_J$ the Stevens coefficients. The magnetic terms in H_M are the Zeeman coupling between the 4f magnetic moments $\boldsymbol{J}$ and the applied magnetic field, $\boldsymbol{H}$, and the Heisenberg-type bilinear interactions, characterized by a θ^* magnetic interaction temperature. Only magnetoelastic contributions linear in strain and restricted to second-rank terms are considered here. They read in symmetrized strains ε^μ as [20]:

$$H_{ME} = -(B^{\alpha 1}\varepsilon^{\alpha 1} + B^{\alpha 2}\varepsilon^{\alpha 2}) O_2^0 - B^\gamma \varepsilon^\gamma O_2^2 - B^\delta \varepsilon^\delta P_{xy} - B^\varepsilon (\varepsilon_1^\varepsilon P_{zx} + \varepsilon_2^\varepsilon P_{yz}) \tag{3}$$

where B^μ are the magnetoelastic coefficients, $P_{ij} = 1/2(J_i J_j + J_j J_i)(ij = xy, yz, zx)$ and the relation between ε^μ and the Cartesian components ε_{ij} is presented in [8]. Within the MFA, the two-ion quadrupolar terms read as:

$$H_Q = -K^\alpha \langle O_2^0 \rangle O_2^0 - K^\gamma \langle O_2^2 \rangle O_2^2 - K^\delta \langle P_{xy} \rangle P_{xy} - K^\varepsilon [\langle P_{yz} \rangle P_{yz} + \langle P_{zx} \rangle P_{zx}]. \tag{4}$$

Note that the γ and δ magnetoelastic modes in equations (3) and (4) correspond to the orthorhombic deformations of the tetragonal crystal structure along [100] and [110] axes, respectively, and the α- and ε-modes correspond to the tetragonal and monoclinic ones, which appear either at the external magnetic field or in the quadrupolar ordered phase. The related elastic energy is written as usual using the symmetrized background elastic constants C_0^μ. E_M and E_Q in equation (1) are the bilinear and quadrupolar corrective energies associated with the MFA.

Minimizing the free energy with regard to the strains gives the equilibrium strains ε^μ as functions of the expectation values of the corresponding quadrupolar operators. Replacing these ε^μ makes H_{ME} (equation (3)) indistinguishable from H_Q (equation (4)) and leads to total quadrupolar coefficients:

$$G^\alpha = \frac{(B^{\alpha 1})^2 C_0^{\alpha 2} - 2B^{\alpha 1} B^{\alpha 2} C_0^{\alpha 12} + (B^{\alpha 2})^2 C_0^{\alpha 1}}{C_0^{\alpha 1} C_0^{\alpha 2} - (C_0^{\alpha 12})^2} + K^\alpha \tag{5}$$

$$G^\mu = \frac{(B^\mu)^2}{C_0^\mu} + K^\mu \qquad (\mu = \gamma, \delta, \varepsilon) \tag{5'}$$

which receive contributions from both the one-ion magnetoelastic B^μ and pair quadrupole K^μ interactions. If sufficiently large these interactions G^μ drive the ordering of the corresponding quadrupolar parameter (structural phase transition) and determine the magnetoelastic contribution to various magnetic properties (for details see [8]). Note that in the absence of any external stress in the tetragonal phase, equation (2) reduces to $H_{CEF} - G^\alpha \langle O_2^0 \rangle O_2^0$ due to the α quadrupolar interactions, which leads to a temperature-dependent apparent second-order CEF coefficient and thus to a temperature-dependent level scheme as was observed, for example, in $TbPO_4$ [6]. In the study of any symmetry-lowering mode, the G^α term has to be previously determined and considered into the initial diagonalization.

In insulating systems, the two-ion quadrupolar terms originate from electric quadrupole–quadrupole interactions and phonon coupling via optical and acoustic phonons [2, 21]. The acoustic contribution to the pair interaction coefficient K^μ is negative and when it dominates a relation $K^\mu / G_{ME}^\mu = -1/3$ is deduced between the magnetoelastic and pair contributions, $G_{ME}^\mu = (B^\mu)^2 / C_0^\mu$ and K^μ, respectively. This ratio appears as a general feature for the most of R zircons [2, 21, 22].

In the presence of small external stresses, perturbation theory can be applied to the disordered phase and the analytical expressions for the free energy and for the magnetoelastic contribution to relevant physical properties can be obtained for different symmetry-lowering modes [8]. For example, the third-order magnetic susceptibility, i.e. the coefficient of the H^3-term in the field expansion of the magnetization depends on four single-ion susceptibilities and receives contributions from both the α- and the γ- (δ-) modes for H along the [100] ([110]) axis:

$$\chi_M^{(3)} = \frac{1}{(1-n\chi_0)^4}\left[\chi_0^{(3)} + \frac{2G^\alpha(\chi_\alpha^{(2)})^2}{1-G^\alpha\chi_\alpha} + \frac{2G^\mu(\chi_\mu^{(2)})^2}{1-G^\mu\chi_\mu}\right]. \tag{6}$$

The single-ion susceptibilities χ_0 and $\chi_0^{(3)}$ describe the magnetic responses proportional to H and H^3 in the absence of any magnetic interaction. The susceptibilities $\chi_\mu = \langle O_2^\mu\rangle/\varepsilon^\mu$ and $\chi_\mu^{(2)} = \langle O_2^\mu\rangle/H^2$ characterize the responses of the Q_μ quadrupolar component to the associated strain and to an applied magnetic field, respectively. The single-ion susceptibilities are deduced immediately from the CEF levels and eigenfunctions (see [8]) and all of them except for χ_0 are anisotropic within the basal plane because they concern different quadrupolar components.

The strain induced in the disordered phase by a magnetic field includes the renormalization of the applied field by the bilinear interactions and of the quadrupolar response by the quadrupolar pair interactions:

$$\varepsilon^\mu = \frac{B^\mu}{C_0^\mu}\frac{\chi_\mu^{(2)}}{(1-n\chi_0)^2(1-G^\mu\chi_\mu)}H^2. \tag{7}$$

Different sets of experimental configurations allow us to separately study the α, γ, δ and ε modes and to determine the corresponding magnetoelastic and pair interaction coefficients. From an experimental point of view, the initial step is the knowledge of the CEF, which determines the single-ion susceptibilities. The fit of $\chi_M(T)$ along the [001] axis and in the basal plane provides us with the bilinear coefficient, θ^*. The temperature variations of $\chi_M^{(3)}$ and $H/(\varepsilon^\mu)^{1/2}$ subsequently give the different pairs of B^μ and K^μ coefficients.

3. Samples and experimental techniques

The well known method of spontaneous crystallization from the solution in the melt was used to grow the single crystals of RPO_4 (R = Tb–Tm) with a PbO–PbF_2–PbP_2O_6–H_3BO_3 melt as a solvent. The crystals were transparent and slightly coloured; their length was about 2–3 mm in each direction of the crystallographic cell. The magnetization measurements were performed using magnetometers in steady magnetic fields up to 10 T and in the temperature range 1.6–300 K. Temperature was regulated within a ± 0.01 K range and the accuracy on the magnetization was around 0.02 μ_B. Magnetostriction deformations were measured by resistive strain gauges both parallel and perpendicular to the external magnetic field, which pointed along one of the principal symmetry axes of the crystal. Magnetostriction data have been collected in fields up to 5 T and in temperatures from 1.5 to 250 K. The absolute accuracy of magnetostriction measurements was about 2×10^{-7} in the liquid-helium temperature range and increased up to 10^{-6} at high temperatures.

4. The crystalline electric field

Today there exist numerous studies of the CEF interactions in the series of R phosphates by different techniques. Optical absorption spectra in $HoPO_4$ have been measured by Bischoff

et al [3] and Enderle *et al* [23]. The crystal-field splitting of the Er^{3+} ground multiplet in $ErPO_4$ was investigated by optical absorption and both non-resonance and resonance Raman scattering [24]. Loong *et al* have recently initiated a systematic studies of magnetic excitations in the stoichiometric RPO_4 series (Tb–Tm) using neutron spectroscopy [18, 25–27]. In comparison with light scattering, this technique directly provides one with information on the splitting of the Russell–Saunders ground state multiplet. However, although the neutron spectra are relatively easy to analyse in terms of magnetic dipole matrix elements, the set of the five CEF parameters present in tetragonal symmetry is not unique and the knowledge of the actual solution has required an analysis in close connection with the light scattering data. Since the susceptibility formalism is used to analyse thermodynamical properties below room temperature, it is developed within the hypothesis of zero intermultiplet mixing; the above CEF parameters have then to be slightly modified. Indeed, the direct use of the values from the literature leads to level spacings slightly different and to thermal variations of the different one-ion susceptibilities not in perfect agreement with the experimental ones (see [7] for details of the procedure).

The best fits to our magnetic data for Dy, Ho and Er phosphates shown in figure 1 have been obtained with the CEF parameters listed in table 1; for completeness the CEF parameters for Tb and Tm phosphates are also given. Note that the uncertainties associated with the parameters are around 5 K and the influence of small shifts of the V_m^1 on the various susceptibilities used in the analyses of magnetic and magnetostriction data have been systematically tested in the following fits.

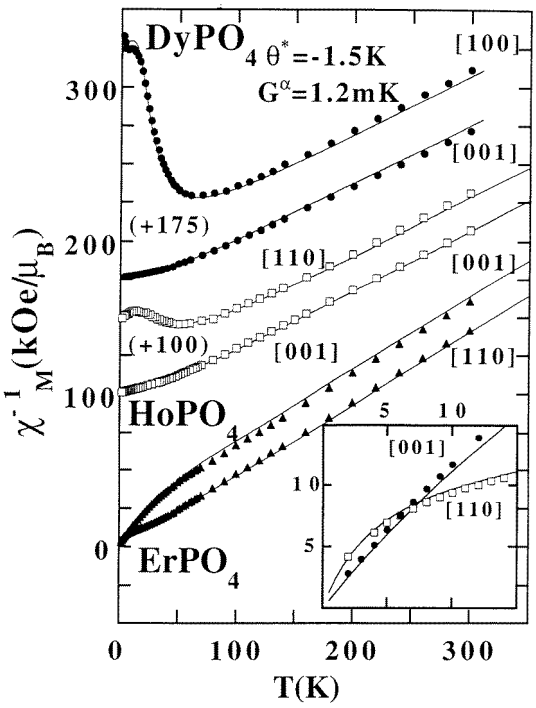

Figure 1. The temperature dependences of the reciprocal first-order susceptibility along the [001] axis and in the basal plane in $DyPO_4$, $HoPO_4$ and $ErPO_4$. $HoPO_4$ and $DyPO_4$ data are shifted upwards by 100 and 175 kOe μ_B^{-1}, respectively. The lines are variations calculated with ($DyPO_4$) and without ($HoPO_4$, $ErPO_4$) bilinear and quadrupolar interactions. The inset gives the low temperature data for $ErPO_4$.

Table 1. CEF parameters for the RPO_4 series derived from neutron spectroscopy (N), and our (M) investigations. The sets of CEF parameters M are used for Dy, Ho and Er phosphates hereafter.

RPO_4	Method	V_2^0(K)	V_4^0(K)	V_4^4(K)	V_6^0(K)	V_6^4(K)
$TbPO_4$ [26]	N	257	22	1203	−71	122
$TbPO_4$ [6]	M	266	37	1246	−52	126
$DyPO_4$ [27]	N	222	18	1080	−66	26
$DyPO_4$	M	202	22	1024	−57	15
$HoPO_4$ [18]	N	289	7	1029	−64	53
$HoPO_4$	M	265	4	956	−60	54
$ErPO_4$ [18]	N	201	28	1143	−48	144
$ErPO_4$	M	250	5	1074	−60	72
$TmPO_4$ [25]	N	227	40	1003	−63	75
$TmPO_4$ [7]	M	258	47	989	−67	60

5. Magnetic susceptibilities

5.1. First-order magnetic susceptibility

Isothermal magnetization curves were collected along the [001], [100] and [110] directions. The first-order magnetic susceptibility was deduced from the M/H versus M^2 plots: the zero-magnetization extrapolation of these plots provides us with the magnetic susceptibility, the initial slope with the third-order one. Magnetic susceptibility in the basal plane is found to be isotropic within the experimental accuracy. A large anisotropy of the first-order susceptibility for Ho and, especially, Dy phosphates is observed in favour of the tetragonal axis, in particular at low temperature (figure 1). In contrast, for Er phosphate in the high temperature range the anisotropy of the χ_M varies in favour of the basal plane in agreement with the change in sign of the second-order Stevens parameter α_J across the R series. Whereas the anisotropy of Er phosphate induced by V_0^2 is large enough at high temperature, cancellation effects due to the high-order CEF terms progressively reduce the anisotropy of the magnetic susceptibility at low temperature.

For all the R phosphates investigated, the variations are close to a Curie–Weiss law above 100 K, with slopes slightly different along the c- and a-axes, which indicates CEF effects still present at room temperature. The temperature dependences of the susceptibility χ_M for $DyPO_4$ and $HoPO_4$ are similar. As temperature decreases, the magnetic susceptibility along the tetragonal axis increases monotonically, whereas in the basal plane it exhibits a broad maximum around 60 and 50 K and decreases rapidly resulting in a huge anisotropy at 4 K of about 280 and 70 for Dy and Ho phosphates, respectively. For these two phosphates, a Van Vleck behaviour is observed in the basal plane resulting in the $\chi_M(T)$ saturation at low temperature. Note the susceptibilities calculated in the basal plane for Dy and Ho phosphates are systematically smaller than the experimental ones below 5 K: this is the signature of a slight misorientation, which reintroduces a contribution to the measured value from the c-axis. Our estimations show that a misorientation of about 1–2° may result in the observed increase of the χ_M along the hard axis. In $ErPO_4$ $\chi_M(T)$ increases monotonically with temperature along [001] and [110] axes and the easy magnetization direction changes from the [001] axis at high temperature to the basal plane around 7.5 K, which is perfectly described by our CEF calculations.

Bilinear interactions are very small for the three RPO_4 investigated here: the effects of a bilinear interaction temperature, ranging from −2 to 2 K, are less active than a variation of the V_m^1 within their uncertainty range, except for $DyPO_4$. Therefore the bilinear exchange

temperatures are taken as zero for Ho and Er phosphates and $\theta^* = -1.5$ K for the Dy one in the following.

5.2. Third-order magnetic susceptibility

The $\chi_M^{(3)}$ temperature dependences for Dy, Ho and Er phosphates are drawn in figures 2–4. For the three compounds, the $\chi_M^{(3)}$-values along the easy magnetic axis are strongly negative at low temperature, which corresponds to magnetization curves without inflection points. Short-range order effects are observed in the $\chi_M^{(3)}$ curves at low temperatures for Dy phosphate and to a much lesser degree for the Ho one. In Dy phosphate, the susceptibility $\chi_M^{(3)}$ in the basal plane is positive, very weak (about 1000 times weaker than that along the [001] axis) and exhibits a broad maximum around 30 K for both [100] and [110] axes. The values of the quadrupolar interaction constants $G^\gamma = 3$ mK and $G^\delta = 12$ mK are derived for $DyPO_4$ from our magnetic data. According to the values of the corresponding α-susceptibilities, the effect of the α quadrupolar interactions is expected to be noticeable in $DyPO_4$; however the quadrupolar constant $G^\alpha = 1.2$ mK derived from parastriction measurements (next section) does not alter significantly the behaviours along the [001] axis and in the basal plane.

For $HoPO_4$ (figure 3), along the c-axis, the fit is less sensitive to the α quadrupolar interactions determined in the following section than to bilinear interactions, even weak. The $\chi_M^{(3)}$ dependences are different along the two principal symmetry axes in the basal plane.

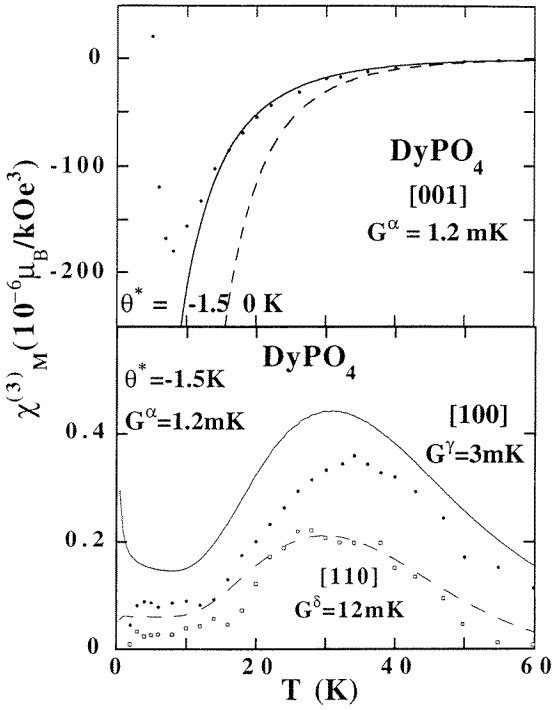

Figure 2. The temperature variations of the third-order susceptibility along the [001] axis (upper part) and in the basal plane (lower part; [100] axis, solid dots; [110] axis, open dots) in $DyPO_4$. The lines are calculated with the bilinear and quadrupolar parameters indicated.

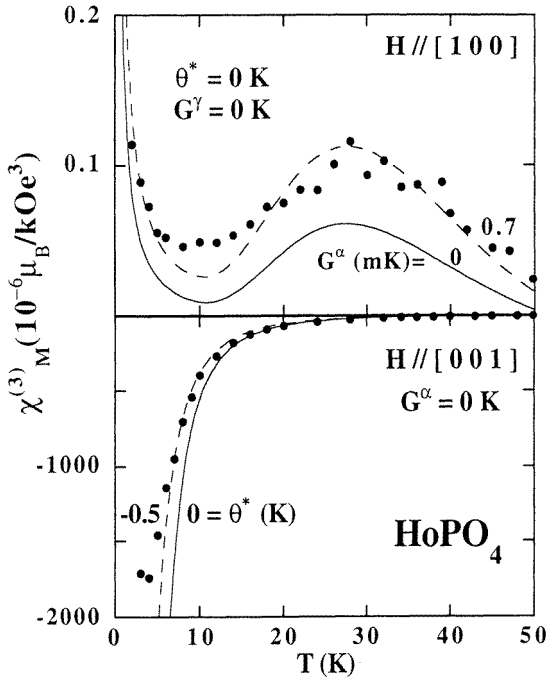

Figure 3. The temperature variations of the third-order susceptibility along the [001] (lower part) and [100] (upper part) axes in $HoPO_4$. The solid curves are calculated with only the crystalline electric field contribution; the dashed curves result from calculations also including quadrupolar and/or bilinear interactions as indicated.

Along the [100] axis $\chi_M^{(3)}$ is very weak (lower than 10^{-7} μ_B kOe^{-3}), positive and exhibits a broad maximum around 30 K and a sharp increase below 4 K. The experimental data are well described by the CEF susceptibility when including either $G^\alpha = 0.7$ mK or $G^\gamma = 8$ mK; whereas the G^α value is coherent with the parastriction determination, the latter value appears too high for the γ-mode (see section 7). Along the [110] axis, $\chi_M^{(3)}$ is measured as very weak and negative in close agreement with the calculated variation, except at low temperature, which could be due to misorientation contributions. In $ErPO_4$ (figure 4), the susceptibility $\chi_M^{(3)}$ is negative along the three directions; it is almost isotropic in the basal plane, about ten times smaller than along the tetragonal axis; fits lead to quadrupolar interactions negligible within the accuracy of the present data.

6. Parastriction measurements

To study the different normal strain modes, the magnetic field was applied successively parallel to the [001], [100] and [110] crystallographic directions. In each case, gauges were glued along the [001] and [100], [100], [010] and [001] and [110] and [$\bar{1}$10], directions, respectively. Linear combinations of the changes of the length measured parallel and perpendicular to the magnetic field lead to the normal modes [8]. The isothermal data are plotted against the square of the field to derive the temperature dependence of their initial slope ε^μ/H^2 which has then to be compared to the predictions from the susceptibility formalism.

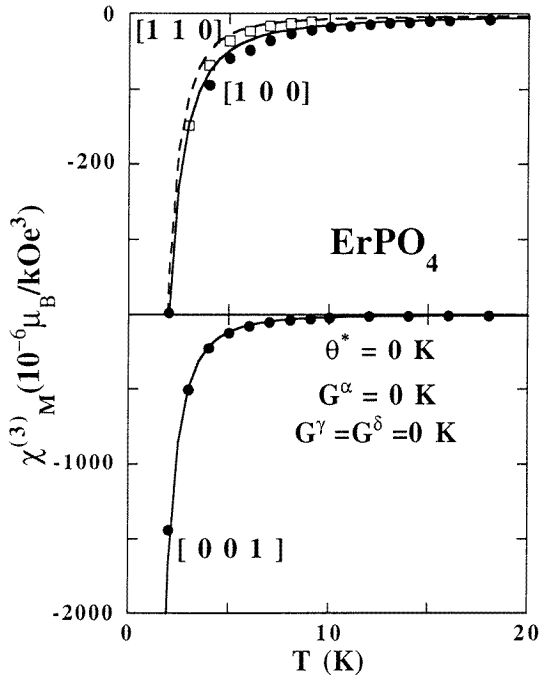

Figure 4. The temperature variations of the third-order susceptibility along the [001] axis (lower part) and in the basal plane (upper part; [100] axis, solid dots; [110] axis, open squares) in $ErPO_4$. The curves are calculated with only the crystalline electric field contribution.

6.1. The α-mode

This mode is usually smaller than the symmetry-lowering modes but is quite noticeable for R zircons as observed in Tb and Tm phosphates [6, 7]. As it concerns the $\langle O_0^2 \rangle$ quadrupolar component already ordered by the CEF and consists of two contributions (bulk variation and change of the c/a-ratio), it is also more difficult to study thoroughly. It is here observed under two experimental conditions, H parallel to the [001] and [100] directions. From $\lambda_{[001]}$ and $\lambda_{[100]}$ measured along [001] and [100] axes, respectively, one obtains for H parallel to [001] [8]:

$$\frac{H}{|\lambda_{[001]} + 2\lambda_{[100]}|^{1/2}} = \sqrt[4]{1/3}\frac{1}{(A^{\alpha 1})^{1/2}}\frac{1}{(\chi_\alpha^{(2)})^{1/2}}[1 - n\chi_0][1 - G^\alpha \chi_\alpha]^{1/2} \quad (8)$$

$$\frac{H}{|\lambda_{[001]} - \lambda_{[100]}|^{1/2}} = \sqrt[4]{2/3}\frac{1}{(A^{\alpha 2})^{1/2}}\frac{1}{(\chi_\alpha^{(2)})^{1/2}}[1 - n\chi_0][1 - G^\alpha \chi_\alpha]^{1/2} \quad (8')$$

For H parallel to the [100] axis one has to change $\lambda_{[100]}$ by $(\lambda_{[100]} + \lambda_{[010]})/2$. The magnetoelastic coefficients $B^{\alpha 1}$ and $B^{\alpha 2}$ can be determined from the experimental $A^{\alpha 1}$ and $A^{\alpha 2}$ constants when knowing the background elastic constants:

$$B^{\alpha 1} = A^{\alpha 1}C_0^{\alpha 1} + A^{\alpha 2}C_0^{\alpha 12} \qquad B^{\alpha 2} = A^{\alpha 1}C_0^{\alpha 12} + A^{\alpha 2}C_0^{\alpha 2}. \quad (9)$$

The experimental temperature variations for $DyPO_4$ are drawn in figure 5 (on the left, $H \parallel [001]$; on the right, $H \parallel [100]$). The best accuracy is obtained for the c-axis data, due to the fact that they are less sensitive to misorientations of the field and the gauge

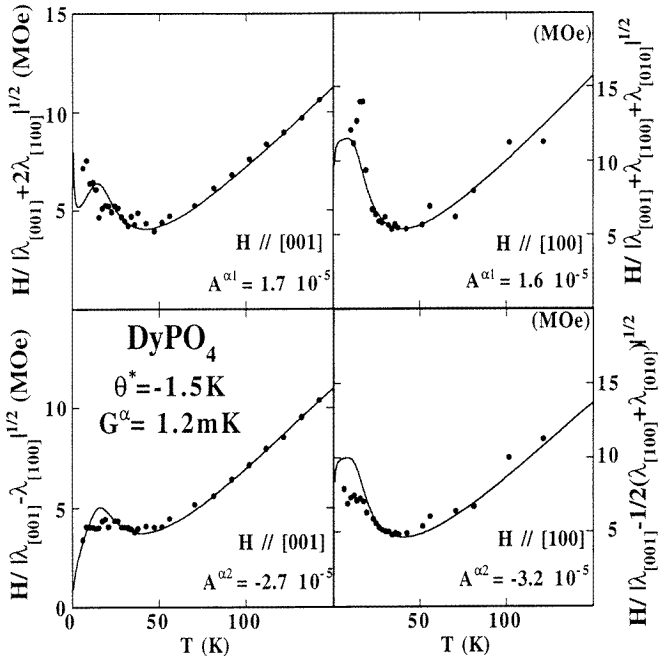

Figure 5. The temperature variations of the parastriction within the α-symmetry for [001] (left panel) and [100] (right panel) magnetic fields (upper part: $\alpha 1$-mode; lower part: $\alpha 2$-mode) in $DyPO_4$. Curves are calculated with bilinear and quadrupolar interactions.

than those for a direction within the basal plane. For the two field orientations [100] and [001], the derived constants $A^{\alpha 1}$ and $A^{\alpha 2}$ are very close, which proves the coherency of the determinations. The corresponding constants $A^{\alpha i}$ for all the phosphates investigated are collected in table 2; in $HoPO_4$, both the $A^{\alpha i}$ and the α-susceptibilities are small and to determine the magnetoelastic coefficients was only possible for a magnetic field along the c-axis; in $ErPO_4$, the α-contributions were too weak to be determined. We have checked that the values of $A^{\alpha 1}$ and $A^{\alpha 2}$ do not depend significantly on the set of CEF parameters chosen. In the case of $DyPO_4$ introducing the bilinear interaction coefficient does not affect the fit, whereas the quadrupolar constant $G^{\alpha} = 1.2$ mK (see below) introduced in the diagonalization improves it slightly.

Going from $A^{\alpha 1}$ and $A^{\alpha 2}$ to $B^{\alpha 1}$ and $B^{\alpha 2}$ requires the knowledge of the α background elastic constants, which were assumed earlier to be $C_0^{\alpha 1} = 2.4$, $C_0^{\alpha 2} = 1.1$, $C_0^{\alpha 12} = 0.16$ in units of 10^6 K [6]. This leads to the $B^{\alpha 1}/\alpha_J$ and $B^{\alpha 2}/\alpha_J$, values normalized by the second-order Stevens parameters, indicated in table 2, and allows us to estimate the magnetoelastic contribution G^{α}_{ME} and the total quadrupolar constant G^{α} assuming the ratio $K^{\alpha}/G^{\alpha}_{ME} = -1/3$. The consequences of the G^{α} coefficient for the various susceptibilities associated with the various symmetry modes have been evaluated. We have checked that changing the G^{α} coefficient in reasonable limits in the fit of the experimental third-order susceptibilities (see equation (6)) does not change significantly the values of the parameters determined in section 5.

In summary, we have obtained experimental evidence for the existence of α magnetoelastic couplings for all of the R phosphates, except $ErPO_4$, and the $A^{\alpha 1}$-, $A^{\alpha 2}$-coefficients have been coherently determined. Since not all the background elastic constants are known, only an

Table 2. Magnetoelastic coefficients $B^{\alpha i}/\alpha_J$ and B^{μ}/α_J normalized by the second-order Stevens coefficients α_J and the magnetoelastic contributions G^{α}_{ME} and G^{μ}_{ME} to the total pair quadrupolar constants for the full symmetry ($\alpha i = \alpha 1,\ \alpha 2$) and symmetry lowering ($\mu = \gamma,\ \delta,\ \varepsilon$) modes, respectively, in rare-earth phosphates RPO_4. $A^{\alpha i}$ are the experimental constants determined by equation (8).

R	$H \parallel [hkl]$; α, μ modes	$A^{\alpha 1}$ (10^{-6})	$A^{\alpha 2}$ (10^{-6})	$B^{\alpha 1}/\alpha_J$ (10^3 K)	$B^{\alpha 2}/\alpha_J$ (10^3 K)	G^{α}_{ME} (mK)	B^{μ}/α_J (10^3 K)	G^{μ}_{ME} (mK)
Tb	[001]; α	32	−47	−6.8	4.6	4.4		
	[100]; α	32	−47					
	[100]; γ						9.9	10
	[110]; δ						−14.4	100
	[101]; ε						2.6	1
Dy	[001]; α	17	−27	−5.5	4.7	1.5		
	[100]; α	16	−32					
	[100]; γ						10.4	4.4
	[110]; δ						−9.3	16.6
Ho	[001]; α	8	−20	−6.1	9.3	0.5		
	[100]; γ						11.3	0.6
	[110]; δ						−11.1	3
Er	[100]; γ						9.8	0.6
	[110]; δ						−13.8	5.8
Tm	[001]; α	−32	47	−6.8	4.6	4.4		
	[100]; γ						7.7	6
	[110]; δ						−14.9	123

estimate of G^{α}_{ME} and of the values of the magnetoelastic coefficients themselves, $B^{\alpha 1}$ and $B^{\alpha 2}$, is proposed here, which, fortunately, does not sizeably modify the different susceptibilities investigated.

6.2. The symmetry-lowering modes

The γ symmetry-lowering mode is obtained from the difference between $\lambda_{[100]}$ and $\lambda_{[010]}$ for $H \parallel [100]$. The negative sign of this difference and the positive value of $\chi^{(2)}_{\gamma}$ indicate the magnetoelastic coefficient to be negative for Dy and Ho phosphates. The relatively weak value of ε^{γ} limits the temperature range investigated to below 150–200 K (figure 6, upper part). The adjustment of the experimental and calculated dependences leads, using $C^{\gamma}_0 = 10^6$ K, an average value in the RVO_4 isomorphous series, to $B^{\gamma} = -66$ K and $B^{\gamma} = -25$ K for Dy and Ho phosphates, respectively [6]. The effects of non-zero G^{γ} coefficients are significantly reduced due to the small magnetoelastic contribution G^{γ}_{ME} (see equation (7)) and the weak χ_{γ}-susceptibility; thus they do not introduce any significant shift in the parastriction curve both for Dy and Ho phosphates. In $ErPO_4$, the magnetoelastic coupling is confirmed, for this symmetry also, to be weak ($B^{\gamma} = 25$ K).

The δ symmetry-lowering mode is obtained from the difference between $\lambda_{[110]}$ and $\lambda_{[\bar{1}10]}$ for $H \parallel [110]$. Due to the positive value of $\chi^{(2)}_{\delta}$ the sign of this difference determines the magnetoelastic coefficient signs which are found to be positive for Dy and Ho phosphates and negative for the Er one. Only data for $DyPO_4$ are presented here (figure 6, lower

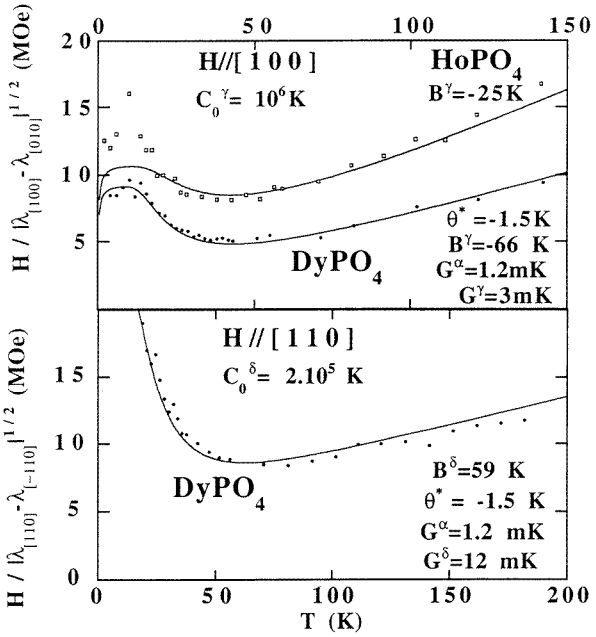

Figure 6. The temperature variations of the parastriction within the γ-symmetry for $DyPO_4$ and $HoPO_4$ (upper part) and the δ-symmetry for $DyPO_4$ (lower part). The lines are calculated with the parameters indicated.

part). The comparison between the calculated and experimental slopes for $DyPO_4$ leads to a magnetoelastic coefficient, $B^{\delta} = 59$ K, using a background elastic constant $C_0^{\delta} = 2.1 \times 10^5$ K, a value estimated as previously from the study of RVO_4 and $TmPO_4$ [21]. For $DyPO_4$, the magnetoelastic coefficients B^{γ} and B^{δ} are comparable in value, although opposite in sign. However the magnetoelastic contribution $G_{ME}^{\delta} = 17$ mK for the δ-mode exceeds about fivefold that for γ-symmetry $G_{ME}^{\gamma} = 4.4$ mK, which is mainly due to the C_0^{δ} value, about one-fifth of the C_0^{γ} one. For this mode also, G^{δ} is small enough not to significantly alter the fit of the data. In $HoPO_4$ and $ErPO_4$, the following values were obtained: $B^{\delta} = 25$ K and $B^{\delta} = -35$ K, respectively, leading to small G^{δ}-values.

Note that the last magnetoelastic mode, associated with the ε-symmetry, was studied in $TbPO_4$ [6]. Usually weak, it does not manifest itself through sizeable softening of the C_{44} elastic constant in the studies devoted to RXO_4 [21]. Data have been collected with a magnetic field applied along the [101] axis and gauges along [101] and [$\bar{1}$01]. Their temperature dependence was then compared to the calculated one which led to $B^{\varepsilon} = -26$ K using a background elastic constant $C_0^{\varepsilon} = 2C_{44}^0 = 7.8 \times 10^5$ K. This large C_{44}^0-value gives small quadrupolar interactions ($G_{ME}^{\varepsilon} \leqslant 1$ mK) and a $B^{\varepsilon}/\alpha_J = 2.6 \times 10^3$ K normalized value, clearly smaller than the values for the γ- and δ-modes; this proves that the hypothesis of neglecting this mode is usually justified.

7. Discussion

The question of the origin of the magnetoelastic couplings in R oxides is identical to the problem of the origin of the CEF itself, which is well known to result from the competition between

numerous antagonistic contributions. Their analysis requires a reliable determination of both the CEF parameters and the magnetoelastic interaction coefficients for the different symmetry modes across a series. Note that generally, due to the experimental uncertainty, it is not very easy to determine an unique set of V_m^1 parameters in the case of tetragonal symmetry, especially when using a single experimental technique. Our sets of the CEF parameters describe closely magnetic data of RPO_4 (R = Tb–Tm) and remain in good agreement with those determined by Loong *et al* [18, 27] (table 1). The analysis of the CEF parameters observed in $HoVO_4$ ($V_2^0 = -126$ K, $V_4^0 = 55$ K, $V_4^4 = 1105$ K, $V_6^0 = -62$ K and $V_6^4 = -112$ K) reveals they are very reminiscent of the RPO_4 values except the second-order one, V_2^0, which is of opposite sign.

No successful theory for the CEF in RE oxides which would derive the reliable CEF parameters from the first principles exists at present. Therefore some experimental regularities in the variation of the CEF parameters across the RPO_4 series which may be observed in the systematic studies is of evident interest. The relative variation of the CEF parameters $\Delta V_m^1/V_m^1$ of different orders for RPO_4 is shown in figure 7. The variation of the V_2^0, V_6^0, and V_4^4 parameters across the series does not exceed 20–30%, whereas the V_4^0 one changes noticeably about 1.5–2 times. It may be checked in table 1 that the relative variation of the V_6^4 coefficient is also large; in this latter case it could be due to a lesser sensitivity of the measured physical properties to this parameter as it looks likely to be from our fits.

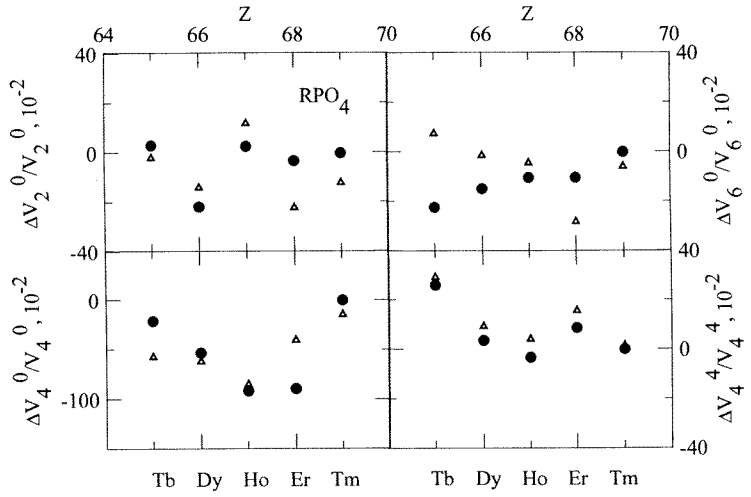

Figure 7. The relative variations of the CEF parameters in the series of RPO_4 (open triangles are from the neutron spectroscopy; full dots are our data). The CEF parameters for $TmPO_4$ are used to normalize the data $\Delta V_m^1/V_m^1 = [V_m^1(\mathrm{R}) - V_m^1(\mathrm{Tm})]/V_m^1(\mathrm{Tm})$.

One can compare the observed variations of the CEF parameters with those expected for different models. According to the well known procedure developed by Morrison and Leavitt for the doped R:LaF_3 the $\Delta_m^1 V/V_m^1$ depend directly on the 4f shell expansion: $\Delta V_m^1/V_m^1 \sim \Delta\rho_m/\rho_m$ with $\rho_m \sim \langle r^m\rangle_{HF}(1-\sigma_m)$; $\langle r^m\rangle_{HF}$ and σ_m are the average radial integrals and the linear screening factors, respectively [28]. Variations of $\Delta\rho_m/\rho_m$ not exceeding ~5% for $m = 2$ and ~20–25% for $m = 4$, 6 were estimated for the series of R:LaF_3 from Tb to Yb. The observed variations of the $\Delta V_m^1/V_m^1$ for R phosphates are in rough agreement with these estimations. Note that for the series of doped crystals, only the effect of the contraction of the 4f shell of R ion was taken into account [28] which results in the

monotonic decrease of all the CEF parameters in absolute value from Tb to Yb. For the pure crystals, there also exists the variation of the crystal structure parameters across the R series which can be taken into account in the frame of the superposition model of CEF [29, 30] (that requires the knowledge of the nearest R ion surroundings).

An important result of the present studies is the observation for the RPO_4 series of all the magnetoelastic modes. The α magnetoelastic modes are determined coherently by parastriction measurements in two different experimental geometries. Due to the sizeable quadrupolar parameters G^{α} a pronounced temperature variation of the energy spacings in the disordered phase may be observed (equation (5)) in the case of nearly degenerate spectrum as for instance in $TbPO_4$ [6]. In contrast to the case of R intermetallics [31], the values of the $\alpha 1$ and $\alpha 2$ modes are non-negligible and result, for example, in pronounced thermal expansion anomalies in RPO_4 (Tb–Tm) [32]; accurate measurements at low temperature in $TbPO_4$ may allow one to measure the temperature dependence of the level spacings.

The quadrupolar interactions within the basal plane have been systematically studied in the RPO_4 series by third-order magnetic susceptibility and parastriction measurements. They provide us with the magnetoelastic coefficient B^{μ} and the magnetoelastic contribution, G^{μ}_{ME}, listed in table 2. The magnetoelastic coefficients B^{μ} for γ- and δ-symmetries are comparable in absolute value, whereas the quadrupolar interactions within the γ-symmetry are less active due to the large value of the C_0^{γ} elastic constant. In connection with their one-ion origin, the magnetoelastic coefficients are the strain derivatives of the second-order CEF parameter [31]: $B^{\mu} = -\alpha_J \partial V_0^2 / \partial \varepsilon^{\mu}$. After normalization by the second-order Stevens coefficient, they become as characteristic of the series under consideration as the CEF parameters themselves (figure 8). In spite of the fact that they are the strain derivatives of the second-order CEF parameter, the magnetoelastic coefficients B^{μ}/α_J change only weakly throughout the R series without any systematic variation and appear at least as constant as V_2^0 itself. The hierarchy of the magnetoelastic coefficients of different symmetry remains the same for all the R phosphates under investigation. The magnetoelastic coefficients for the $\alpha 1$- and $\alpha 2$-modes are opposite in sign and comparable in value; this is also true for the γ and δ symmetry-lowering modes for which the magnetoelastic coefficients are about 1.5–2 times larger than the tetragonal ones. It is also possible to compare the magnetoelastic coefficients obtained in $HoVO_4$ by the same

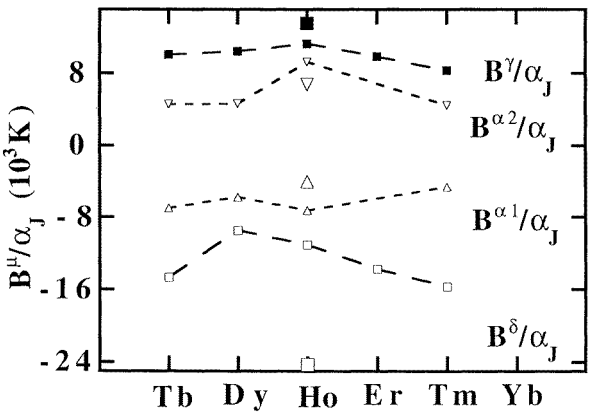

Figure 8. The variations of the magnetoelastic coefficients $B^{\alpha i}/\alpha_J$ and B^{μ}/α_J normalized by the second-order Stevens parameters for the full symmetry and symmetry-lowering modes across the series of RPO_4 (large symbols correspond to the values determined in $HoVO_4$).

techniques ($B^{\alpha 1}/\alpha_J = -4.05$, $B^{\alpha 2}/\alpha_J = 6.76$, $B^{\gamma}/\alpha_J = 13.5$ and $B^{\delta}/\alpha_J = 24.3$ in 10^3 K units) to the RPO_4 values: they are very similar. Thus, although the V_2^0 parameter is opposite in sign in R vanadates and phosphates, its strain derivative keeps, for all the symmetry modes, the same value, which would set a puzzling problem when trying to describe the origin of the one-ion magnetoelasticity using CEF models.

As a consequence, the magnetoelastic contributions, $(B^{\mu})^2/C_0^{\mu}$, to the G^{μ} quadrupolar constants vary as $(\alpha_J)^2$ across the series, i.e. the G_{ME}^{μ} values are the largest for the starting (Tb) and the ending (Tm) members of the series and decrease sharply for Dy and especially Ho and Er phosphates. That is why the spontaneous quadrupolar orderings are observed mostly for Tb, Tm and Dy compounds. Indeed the occurrence of the quadrupolar ordering is governed by the quadrupolar interactions and the CEF level scheme which determines the χ_{μ} susceptibilities. The ordering occurs at a T_Q value given by $1/\chi_{\mu}(T_Q) = G^{\mu}$. For the δ-symmetry, the $1/\chi_{\mu}$-susceptibility exhibits Van Vleck behaviours at low temperature for all the compounds, except $TbPO_4$ (figure 9). In $TbPO_4$, $G^{\delta} = 70$ mK drives the δ orthorhombic ordering around 2.1 K immediately below the Néel temperature. In the other RPO_4, the G^{δ}-values are quite unable to order the $\langle P_{xy} \rangle$ quadrupolar component. As it is not possible to act on the quadrupolar interactions themselves, the only way to drive the $\langle P_{xy} \rangle$ system to criticality is to reconstruct the level spacing and the wavefunctions using an external stress. The cooperative Jahn–Teller effect stimulated by a [100] magnetic field is described in [33]; such a stimulated ordering is not possible in $ErPO_4$.

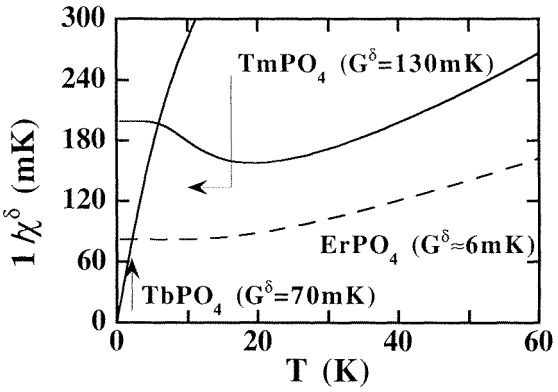

Figure 9. The temperature variations of the reciprocal strain susceptibility within the δ-symmetry in RPO_4. For R = Dy and Ho the values of the reciprocal strain susceptibility are out of the frame. The G^{δ}-values are not able to drive a spontaneous quadrupolar ordering in all the phosphates investigated except for $TbPO_4$.

For the γ-symmetry also, the $1/\chi_{\mu}$-susceptibility exhibits Van Vleck behaviours at low temperature for all the compounds, except $TbPO_4$. In this latter, the $G^{\gamma} = 46$ mK [6] would drive the γ orthorhombic ordering around 1 K, in the absence of the δ orthorhombic ordering. In the other RPO_4, the lowest values of $1/\chi_{\gamma}$ are calculated to be larger than 80 mK, preventing any possibility of a γ orthorhombic ordering.

The systematic determination of the CEF and of the magnetoelastic couplings here realized constitutes a reliable basis for describing these couplings in insulating compounds, with some intriguing problems about the second-order CEF coefficients and their strain dependence. Studies of magnetoelasticity in isomorphous RVO_4 and other oxide compounds and their comparison for different structures are of great interest. Of particular interest is the comparison

of magnetoelastic effects in zircons and scheelites, which both possess tetragonal symmetry, but belong to different crystallographic groups; note that there exist calculations of magnetoelastic coefficients for scheelite-structure crystals [34].

Acknowledgments

The Laboratoire Louis Néel is Unité Associée à l'Université Joseph-Fourier, Grenoble. This research is supported, in part, by the Russian Fundamental Science Foundation. One of us, ZK, wants to thank the Ministère de la Recherche et de la Technologie for its support and the Laboratoire Louis Néel for its hospitality.

References

[1] Wyckoff W G 1965 *Crystal Structure* vol 3 (New York: Interscience) p15
[2] Gehring G A and Gehring K A 1975 *Rep. Prog. Phys.* **38** 1
[3] Bischoff H, Pilawa B, Kasten A and Kahle H G 1991 *J. Phys.: Condens. Metter.* **3** 10 057
[4] Christensen H P 1979 *Phys. Rev.* B **19** 6573
[5] Elchaninova S D and Zvyagin A I 1978 *Fiz. Nizk. Temp.* **4** 1465
[6] Morin P, Rouchy J and Kazei Z 1994 *Phys. Rev.* B **50** 12 625
[7] Morin P, Rouchy J and Kazei Z 1996 *J. Phys.: Condens. Matter.* **8** 7967
[8] Morin P, Rouchy J and Schmitt D 1988 *Phys. Rev.* B **37** 5401
[9] Wright J C and Moos H W 1969 *Phys. Lett.* A **29** 495
[10] Cooke A H, Swithenby S J and Wells M R 1973 *J. Phys. C: Solid State Phys.* **6** 2209
[11] Kockelmann W, Schafer and Will G 1991 *Eur. J. Solid State Inorg. Chem.* **25** 515
[12] Wright J C, Moos H W, Colwell J H, Mangum B W and Thornton D D 1971 *Phys. Rev.* B **3** 843
[13] Jahn I R and Smith S H 1975 *Phys. Status Solidi* b **68** 531
[14] Regis M, Ferre J, Farge Y and Jahn I R 1977 *Physica* B **86–88** 599
[15] Rado G T 1969 *Phys. Rev. Lett.* **23** 644
[16] Laugsch J, Kahle H G, Schwab M and Wuchner W 1975 *Physica* B **80** 269
[17] Neogy D, Harabhusan Sen and Wanklyn B M 1989 *J Magn. Magn. Mater.* **78** 387
[18] Loong C-K, Soderholm L, Hammonds J P, Abraham M M, Boatner L A and Edelstein N M 1993 *J. Phys.: Condens. Matter.* **5** 5121
[19] Stevens K W H 1952 *Proc. Phys. Soc.* A **65** 209
[20] du Tremolet de Lacheisserie E 1970 *Ann. Phys., Paris* **5** 267
[21] Melcher R L 1976 *Physical Acoustics* vol XII, ed W P Mason and R N Thurston (New York: Academic) p 1
[22] Levy P M, Morin P and Schmitt D 1979 *Phys. Rev. Lett.* **42** 1417
[23] Enderle M, Pilawa B and Kahle H G 1990 *J. Phys.: Condens. Matter* **2** 4711
[24] Becker P C, Williams G M, Russo R E, Edelstein N, Koningstein J A, Boatner L A and Abraham M M 1986 *Opt. Lett.* **11** 282
[25] Loong C-K, Soderholm L, Abraham M M, Boatner L A and Edelstein N M 1993 *J. Chem. Phys.* **98** 4214
[26] Loong C-K, Soderholm L, Godman G L, Abraham M M and Boatner L A 1993 *Phys. Rev.* B **48** 6124
[27] Loong C-K, Soderholm L, Simon Xue J, Abraham M M and Boatner L A 1994 *J. Alloys Compounds* **207** 165
[28] Morrison C A and Leavitt R P 1979 *J. Chem. Phys.* **71** 2366
[29] Nekvasil V 1979 *Czech. J. Phys.* B **29** 785
[30] Nekvasil V 1988 *Solid State Commun.* **65** 1103
[31] Morin P and Schmitt D 1990 *Ferromagnetic Materials* vol 5, ed K H J Buschow and E P Wohlfarth (Amsterdam: North-Holland) p 1
[32] Sokolov V I, Kazei Z A and Kolmakova N P 1992 *Physica* B **176** 101
[33] Morin P and Kazei Z 1996 *Phys. Rev.* B **55** 8887
[34] Malkin B Z 1987 *Spectroscopy of Solids Containing Rare-Earth Ions* ed A A Kaplyanskii and R M Macfarlane (Amsterdam: North-Holland) p 13